Electronic Transduction of Proton Translocations in Nanoassembled Lamellae of Bacteriorhodopsin

Gerardo Palazzo,[†,‡,*] Maria Magliulo,[†] Antonia Mallardi,[§] Maria Daniela Angione,[†,∥] Danka Gobeljic,[⊥,△] Gaetano Scamarcio,[⊥] Emiliano Fratini,[‡,⊗] Francesca Ridi,[‡,⊗] and Luisa Torsi[†,‡,*]

[†]Dipartimento di Chimica, Università degli Studi di Bari "A. Moro", Via Orabona, 4, 70126 Bari, Italy, [‡]CSGI (Center for Colloid and Surface Science), Units of Bari and Florence, Italy, [§]CNR-IPCF, Istituto per i Processi Chimico-Fisici, Via Orabona, 4, 70126 Bari, Italy, [⊥]CNR-IFN and Dipartimento Interateneo di Fisica, Università degli Studi di Bari "A. Moro", Via Orabona, 4, 70126 Bari, Italy, and [⊗]Dipartimento di Chimica "Ugo Schiff", Università degli Studi di Firenze, Via della Lastruccia, 3, 50019 Sesto Fiorentino, Italy. M.M. and M.D.A. fabricated the devices and carried out the electrical, optical, and sensing measurements. A.M. prepared and characterized the PM suspensions and discussed the relevant data. E.F. and F.R. performed the GISAXS and AFM experiments. G.S. and D.G. performed the Raman measurements. L.T. and G.P. conceived and wrote the manuscript. [∥]Present address: (M. Daniela) Angione School of Chemistry and Centre for Research on Adaptive Nanostructures and Nanodevices (CRANN), University of Dublin Trinity College, College Green, Dublin, Dublin D2, Ireland. [△]Present address: (D. Gobeljic) Institute for Material Science and Center for Nanointegration Duisburg-Essen (CeNIDE), University of Duisburg-Essen, Universitätsstraße 15, 45141 Essen, Germany.

ABSTRACT An organic field-effect transistor (OFET) integrating bacteriorhodopsin (bR) nanoassembled lamellae is proposed for an in-depth study of the proton translocation processes occurring as the bioelectronic device is exposed either to light or to low concentrations of general anesthetic vapors. The study involves the morphological, structural, electrical, and spectroscopic characterizations necessary to assess the functional properties of the device as well as the bR biological activity once integrated into the functional biointerlayer (FBI)-OFET structure. The electronic transduction of the protons phototranslocation is shown as a current increase in the p-type channel only when the device is irradiated with photons known to trigger the bR photocycle, while Raman spectroscopy reveals an associated C═C isomer switch. Notably, higher energy photons bring the *cis* isomer back to its *trans* form, switching the proton pumping process off. The investigation is extended also to the study of a PM FBI-OFET exposed to volatile general anesthetics such as halothane. In this case an electronic current increase is seen upon exposure to low, clinically relevant, concentrations of anesthetics, while no evidence of isomer-switching is observed. The study of the direct electronic detection of the two different externally triggered proton translocation effects allows gathering insights into the underpinning of different bR molecular switching processes.

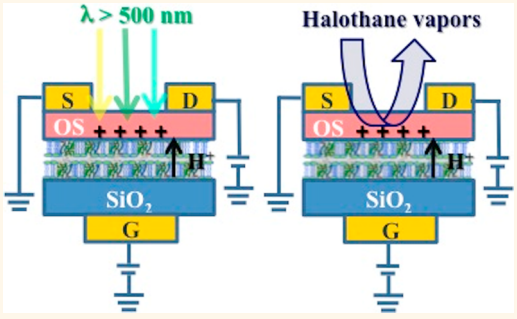

KEYWORDS: organic field-effect transistors · conformational changes · bioelectronic device · bacteriorhodopsin · electronic sensing · self-assembly · proton-pumping mechanism

Bacteriorhodopsin (bR) is a small (~26 kDa) transmembrane protein that transduces light energy into the chemical free energy of a proton gradient occurring across the cell membrane that sustains, *in vivo*, the cell life through ATP synthesis.[1] bR has a rather simple structure consisting of a single polypeptidic chain folded into seven-membrane-spanning α-helices in which a single molecule of retinylidene chromophore (retinal) is covalently bound to a lysine residue of the polypeptide through an imine known as a Schiff base. This is the light-absorbing moiety responsible for initiating a photoinduced proton translocation process.

The overall cycle is initiated as the retinal chromophore absorbs a green-yellow photon ($h\nu$), triggering a rather complicated photocycle.[2] The primary photochemical event involves the isomerization of the retinal from *all-trans* to 13-*cis*, producing the first trappable intermediate state, and it proceeds through several states characterized by different absorbance maxima.[3] The longest living M_{412} intermediate, also characterized by the most blue-shifted absorbance, is the deprotonated Schiff base. When bR proteins are kept dry, the photocycle stops at the *M*-state, before the Schiff base can be reprotonated, due to the shortage of protons. Ultrafast photoinduced charge separation

* Address correspondence to luisa.torsi@uniba.it; gerardo.palazzo@uniba.it.

Received for review March 10, 2014 and accepted July 31, 2014.

Published online July 31, 2014
10.1021/nn503135y

$$bR_{568} \underset{\lambda = 442 \text{ or in the dark}}{\overset{\lambda > 500\ nm}{\rightleftharpoons}} M_{412} + H^+$$

Scheme 1

is therefore followed by a slow charge recombination as the protein returns to its ground state.[4,5] These features allow adopting a simplified model scheme for the dry state, involving the sole switching between the purple bR_{568} and the green-yellow M_{412} states as reported in Scheme 1:[6]

The cycle closes either by leaving the light-adapted bR for few tens of seconds in the dark or by shining blue light on it. In Scheme 1 it is also emphasized how the photoinduced isomerization is associated with the release of a proton.

The bR photocycle involves several molecular switches. At first the photoinduced isomerization of the C13−C14 double bond (isomer switch) occurs; then the deprotonation of the aspartic acid 85 (amino acid protonation switch) takes place, immediately followed by the deprotonation of the Schiff-base linkage (Schiff-base protonation switch), leading to a conformation change of the surrounding protein (conformation switch).[2]

It has been demonstrated that spectral changes akin to those associated with photoinduced proton translocation occur in bR also upon exposure to general anesthetics.[7,8] Such a process is revealed by the occurrence of a shift in the bR absorbance peak. Notably, the proton-pumping capabilities associated with interactions with the anesthetic molecules have been always triggered, so far, by green-yellow light excitation. A photoinduced isomerization eventually occurs, along with the switching process caused by anesthetics, making it difficult to independently investigate the molecular process underpinning the interactions solely with the anesthetics.

In vivo, the direct conversion of photons into chemical energy takes place within specialized patches of the bacterium *Halobacterium salinarum* plasmic membrane known as purple membranes (PMs). bR is the sole protein contained in PM lamellae, where it exists as a highly ordered hexagonal two-dimensional crystalline lattice of uniformly oriented bR trimers with an extremely low phospholipid/protein ratio, which confers exceptional stability against thermal and chemical degradation. These PM patches can be easily isolated from the cell membrane by means of mild procedures, making these membranes a potentially low-cost material, suitable for several applications.[9−13]

PM patches, composed of regularly nanoassembled lamellae of bR proteins, are here integrated into a functional biointerlayer (FBI) organic field-effect transistor (OFET),[14] with PMs forming the interlayer residing between the dielectric and the organic semiconductor. The concept of the FBI-OFET has been recently introduced,[14] and studies on FBIs of phospholipid bilayers[15] or of hydrophilic proteins such as streptavidin or antibodies appeared afterward.[16,17] The first seminal paper also addressed the case of a PM biointerlayer showing preliminary evidence of electron transduction of proton-pumping activity, which calls for a more in-depth investigation. An FBI-OFET configuration foresees a biological interlayer lying at the interface where the OFET two-dimensional transport occurs.[18,19] A direct coupling between the proteins and the transistor channel is eventually established, allowing the electronic probing of subtle changes occurring in the biological layer.[14,20]

In this article a PM FBI-OFET is used to electronically detect the proton translocation effects occurring as the device is exposed either to physical or chemical external stimuli such as light or anesthetic vapors. The study allows us to obtain insights into the molecular switching processes that underpin the two different translocation effects, although both can be associated with a direct electronic/ionic interaction occurring between the PM and the OFET p-type organic semiconductor. To the best of our knowledge it is the first time that the two differently generated proton translocation processes are studied and compared using the same transducing device.

RESULTS AND DISCUSSION

Bacteriorhodopsin and PM FBI-OFET Structure. On the left side of Figure 1A a schematic cross sectional view of the FBI-OFET embedding a PM film is reported. The bioelectronic device holds the structure of a bottom-gate top-contact thin-film transistor sensor.[21,22] The gate contact (G) is interfaced to a 300 nm thick SiO_2 dielectric layer. As typical for FBI-OFETs, the PM interlayer is sandwiched between the dielectric and the organic semiconductor (OS), a regioregular poly(3-hexylthiophene-2,5-diyl) (RR-P3HT) in this case. The source (S) and drain (D) gold top-contacts define a $L = 200\ \mu$m long electronic channel. In the central part of Figure 1A a PM is sketched as discrete lamellae comprising a phospholipid (PL) bilayer embedding a trimer of bR proteins. The highly ordered PM lamellae nanostructure, characterized by an extremely low PL/protein ratio (*ca.* 75% bR and 25% lipid),[13] holds an exceptionally high stability against thermal and chemical degradation.[23] In the rightmost part of Figure 1A a single bR protein is shown with the arrow indicating proton translocation whose direction goes from the cytoplasmic to the extracellular side of the membrane. The core of the photoactive process involves the retinal chromophore, whose chemical structure in the protonated *all-trans*-retinal and deprotonated 13-*cis*-retinal forms is reported in Figure 1B. The conversion of light into metabolic energy occurs

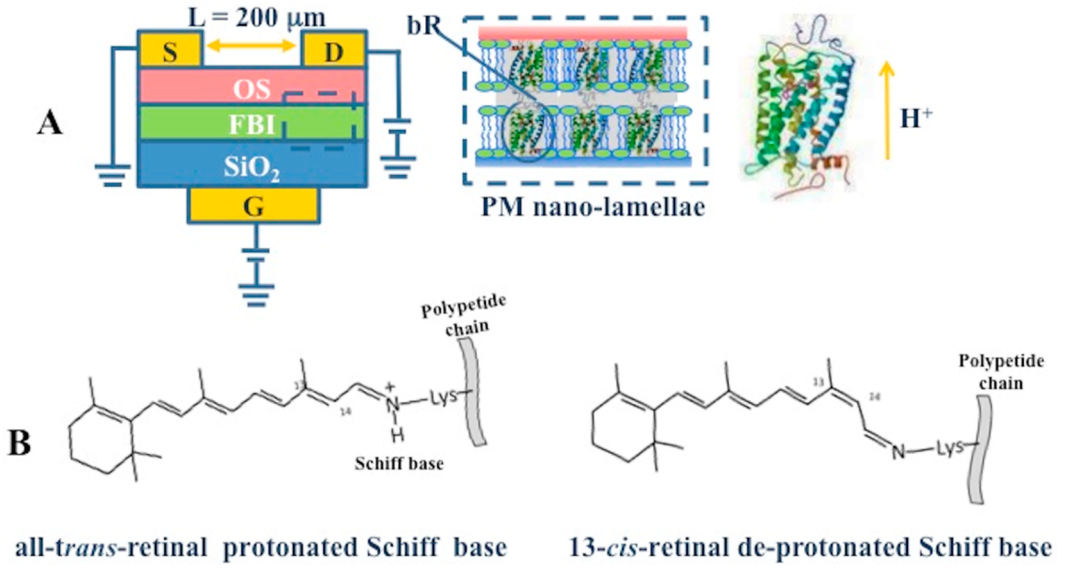

Figure 1. (A) Schematic illustration of the PM FBI-OFET device. A sketch of the purple membrane lamellae is shown along with a drawing of the bacteriorhodopsin protein. (B) Chemical structures of the two conformational states of the retinal chromophore.

because of the bR light-driven ion-pumping activity that translocates protons from the inside to the outside of the bacterial membrane upon illumination. The PM color turns from purple (the bR_{568} form) to green-yellow (the M_{412} form) concomitant with the proton translocation process, according to Scheme 1. Specifically, in the dark the bR molecules within the PMs contain *all-trans* protonated Schiff-base retinal characterized by an absorption at ~568 nm, conferring the characteristic purple color. This bR conformational state is here addressed as bR_{568} or dark adapted. The proton translocation cycle[22] is triggered upon exposure to green-yellow light (λ > 500 nm), and the retinal switches to the deprotonated 13-*cis*-retinal configuration. A steady state characterized by an absorption maximum in the violet-blue region (conferring a green-yellow color) is eventually reached upon continuous illumination; this is here addressed as M_{412} or light-adapted form. The cycle can be closed either by keeping the PM in the dark for a few tens of seconds or by shining blue light (*e.g.*, 442 nm), which immediately brings the M_{412} form back to the bR_{568} one.

PM-P3HT Staked Layers' Nanomorphology and Structure. Before entering into the details of the PM FBI-OFET electronic properties, it is important to assess the PM-P3HT stacked layers' nanomorphology and structure. The atomic force microscope (AFM) image of the P3HT deposited on SiO_2 (Figure 2A) shows a nanostructured morphology formed of granular domains ~100 nm wide, as expected for a regioregular P3HT[24] as well as for other alpha-hexathienylene thin films.[25,26] Figure 2B features a 1 μm thick PM assembly covered by a 20 nm P3HT film. In the staked PM-P3HT system, the nanostructured grains on the surface are ascribable to the covering P3HT layer, while the larger features are attributed, for comparison with blank experiments, to the PM nanolamellae self-assembled underneath. The P3HT porous morphology, constituted of contiguous nanograins, allows volatile molecules to easily percolate through it, reaching the PM layer lying underneath.

The structures of the PM and PM-P3HT layers have been studied by means of the grazing incidence small-angle X-ray scattering (GISAXS) technique, which involves a monochromatic X-ray beam directed at a planar surface with a very small (grazing) incident angle with respect to the sample surface. The radiation scattered by the surface of the sample is then collected by either a 1D or 2D detector. Figure 2C shows the out-of-plane GISAXS scattering coming from both the PM sample (black line) and the PM-P3HT stacking layers (blue line), both deposited on a Si/SiO_2 substrate. The GISAXS curve of the bare P3HT layer, similar to that of the of Si/SiO_2 wafer, is not reported. In the PM and PM-P3HT GISAXS curves the first three orders are visible with a periodicity corresponding to a 1:2:3 type relationship. This proves the occurrence of a one-dimensional lamellar order, with the lamellae oriented parallel to the substrate. The average interlamellar spacing, extracted by a linear interpolation for q_z *vs* $1/2\pi n$ (n = 1, 2, 3 indicating the Bragg reflection order and q_z the value of the scattered vector for the nth reflection) is 5.0 $\pm$ 0.4 nm, in agreement with the thickness reported in the literature for one staked patch of dry PM.[23] The functional biological interlayer is therefore composed by stacks of PM lamellae piled parallel to the SiO_2 surface. The GISAXS curve for the system in which the PMs are deposited beneath the organic semiconductor (PM-P3HT) film shows narrower peaks, which evidence an unchanged lamellar thickness with a better defined interface.

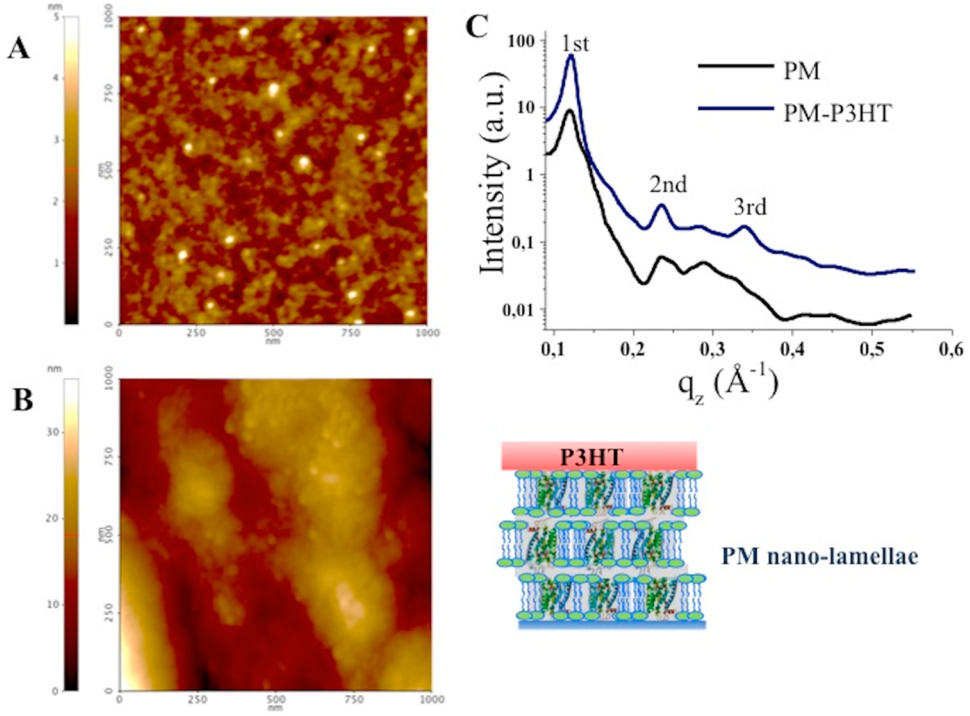

Figure 2. AFM images of a P3HT film (A) and of PM-P3HT staked layers (B) deposited on a SiO_2 surface. For the PM-P3HT system a sketch of the structure is reported on the right. (C) Out-of-plane GISAXS scattering distribution for the PM film and PM-P3HT staked layers.

Taking into account the whole thickness (1 μm) of the PM deposit and each staked nanolamella spacing (5 nm), approximately 200 lamellae constitute the whole PM interlayer in the PM FBI-OFET. In the self-assembled PM layer each nanolamella lies parallel to the SiO_2 surface, but they can be directed upward or downward. Eventually, the bR proteins included in the patches randomly expose the cytoplasmic or the extracellular side to the interface with the P3HT layer and proton pumping is generated in both directions so that, in the absence of an external bias, no net proton photocurrent can be detected.[27]

Bacteriorhodopsin Photoactivity in PM FBI-OFET. Although the PM has been shown to retain its structure upon integration into the FBI-OFET, this does not necessarily imply that the bRs retain their biological functionality. To assess this issue, the bR photoactivity is investigated by studying the changes occurring in the PM-P3HT bilayer spectrum upon green-yellow light ($\lambda > 500$ nm) illumination. The PM-P3HT on a glass substrate is sketched in Figure 3A, while the visible absorption spectra in the dark (meaning the sample exposed to only the spectrometer source light) and under illumination are compared in Figure 3B. The spectrum measured in the dark is dominated by the absorption peak at ~570 nm, ascribed to the bR's *all-trans* retinal (purple line). Upon exposure to a $\lambda > 500$ nm beam, the retinal switches to the 13-*cis*-retinal configuration, triggering the proton translocation cycle. A steady state is eventually reached upon continuous illumination (green line),

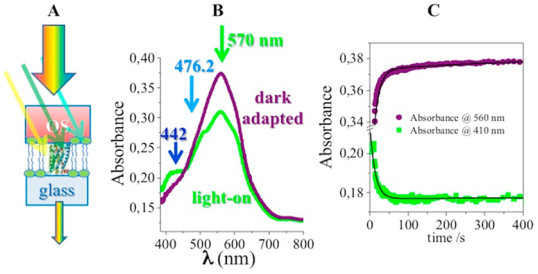

Figure 3. (A) PM-P3HT sample deposited on a glass substrate along with the light exposure conditions. (B) Comparison of the visible absorption spectra in the dark and under illumination. The purple curve is the absorption spectrum of the PM-P3HT measured in the dark, while the green curve is measured under continuous illumination with a halogen lamp filtered through a green-yellow filter ($\lambda > 500$ nm). (C) Recovery kinetics from the bleaching measured at 560 and 410 nm. Dots represent the experimental data, while solid dark lines are the result of a modeling involving the superimposition of two first-order kinetics.

characterized by the presence of a new absorption maximum at 412 nm. The PM-P3HT absorbance spectrum under green-yellow light indeed exhibits a pronounced bleaching in the region 480−650 nm with the appearance of the characteristic fine structure typical of the regioregular P3HT absorption. This result means that, although the P3HT and the bR share the same absorption range, illumination selectively bleaches the bR absorption. Furthermore, illumination induces the rising of a band at 412 nm, associated with the light-adapted form, proving that the bR molecules in the PM interlayer underneath the P3HT film are still capable of

isomer-switching; namely, they are still biofunctional. It can be noted that the fraction of proteins in the light-adapted state under steady-state illumination is ruled by their rate of natural relaxation and the intensity of the exciting beam.

The spectral changes are annulled as the green-yellow light source is switched off. The recovery kinetics from the light-adapted bR form at 560 nm and at 410 nm are shown in Figure 3C. The two processes are parallel and clearly biphasic and can be ascribed to a superposition of two first-order kinetics: a fast process with a characteristic time of 8 ± 1 s and a slower one with a characteristic time of about 98 ± 8 s. Continuous illumination of photoactive proteins in the solid form often results in the trapping of photointermediates.[28,29] Accordingly, slow three-component relaxation after continuous illumination of dry bacteriorhodopsin was previously reported.[5] While the faster process (decay time 1 s) is beyond the limits of our apparatus, the slower components (decay times of ~10 and 100 s) are in very good agreement with the results of Figure 3C. This finding further enforces the idea that the presence of the P3HT layer does not affect the bR functionality. We want to emphasize that all the above-described photoinduced effects are not visible on the bare P3HT layer.

PM FBI-OFET Electrical Characterization. The electrical characterization was performed by operating the devices in the common-source configuration, and typical current–voltage (I_{DS} *vs* V_{DS}) curves at different V_G bias, acquired in the double run mode, are reported in Figure 4A. All the *I*–*V* curves exhibit clearly defined linear and saturated regions as well as current modulation, and a very low leakage current at low source–drain voltage is seen. This shows that the electronic properties of the organic semiconductor (P3HT) remain mostly unchanged as it is deposited on an uneven biological layer. Likely, the flexible P3HT film, composed of contiguous nanograins, smoothly adapts to the uneven PM layer. It is also interesting to underline that the hysteresis evidenced by the recording in the double run mode is negligible. Both these features are remarkable considering that a biosystem is integrated into the device channel region. The electronic parameters (field-effect mobility, μ_{FET}, current amplification, on/off ratio, and threshold voltage V_T) that are critical to define the bioelectronic device performance level were extracted from the experimental current–voltage characteristics using the assessed procedure[30] involving the analysis of the square root of I_{DS} measured in the saturation region, namely, at $V_{DS} = -80$ V, while sweeping the gate bias (Figure 4B). The equation used to extrapolate the parameters is

$$\sqrt{I_{DS}^{SAT}} = \sqrt{\frac{W}{L}\mu_{FET}C_i}(V_G - V_T) \qquad (1)$$

where C_i is the FET dielectric capacitance per unit area, being 12 nF/cm^2, while $L = 200$ μm and $W = 4$ mm are the channel length and width, respectively. The analysis of the data, averaged over 10 samples, is reported in Table 1, showing also a comparison with the data taken from a bare P3HT OFET. Clearly, the mobility is almost unaffected by the PM integration, while the threshold voltage is shifted toward more positive values. This can be explained considering the net negative charge carried by bR proteins effectively acting as an extra gating. The OFET on/off ratio decreases upon integration of the PM probably due to the slight ionic conductivity of the biological layer. Interesting is also that a μ_{FET} and on/off ratio as high as 2×10^{-2} cm^2 V^{-1} s^{-1} and 6×10^3, respectively, could be achieved with a soluble pentacene-based OFET with the PM.[14]

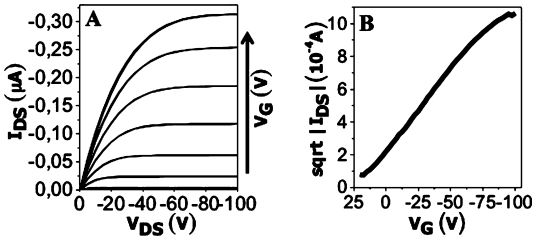

Figure 4. (A) Current–voltage (*I*–*V*) characteristics of a PM FBI-OFET measured in the double run mode. (B) Square root of $|I_{DS}|$ *vs* V_G plots for the same device.

Raman Spectroscopic Investigation of Gate-Biased PM FBI-OFET. The Raman investigation was carried out to independently assess the occurrence of the isomerization of the retinal from *all-trans* to 13-*cis* by directly addressing the changes in the bR C=C stretching vibration peak. To this end, micro-Raman spectroscopy was chosen to probe the PM FBI-OFET under light or under halothane, as well as while the PM FBI-OFET device was subjected to a gate bias. To acquire the

TABLE 1. Figures of Merit Extracted from the PM FBI-OFETs and Bare P3HT-OFET *I*–*V* Curves[a]

	P3HT-OFET		PM FBI-OFET	
	av (n = 10)	best	av (n = 10)	best
μ_{FET} (cm^2 V^{-1} s^{-1})	(2.8 ± 0.79) × 10^{-3}	4.0 × 10^{-3}	(1.28 ± 0.28) × 10^{-3}	2.7 × 10^{-3}
V_T (V)	7.7 ± 3	5.5	17 ± 7	7
on/off	1168 ± 310	1890	181 ± 40	237

[a] Values are expressed as the average over 10 replicates, and errors are the relevant standard deviations.

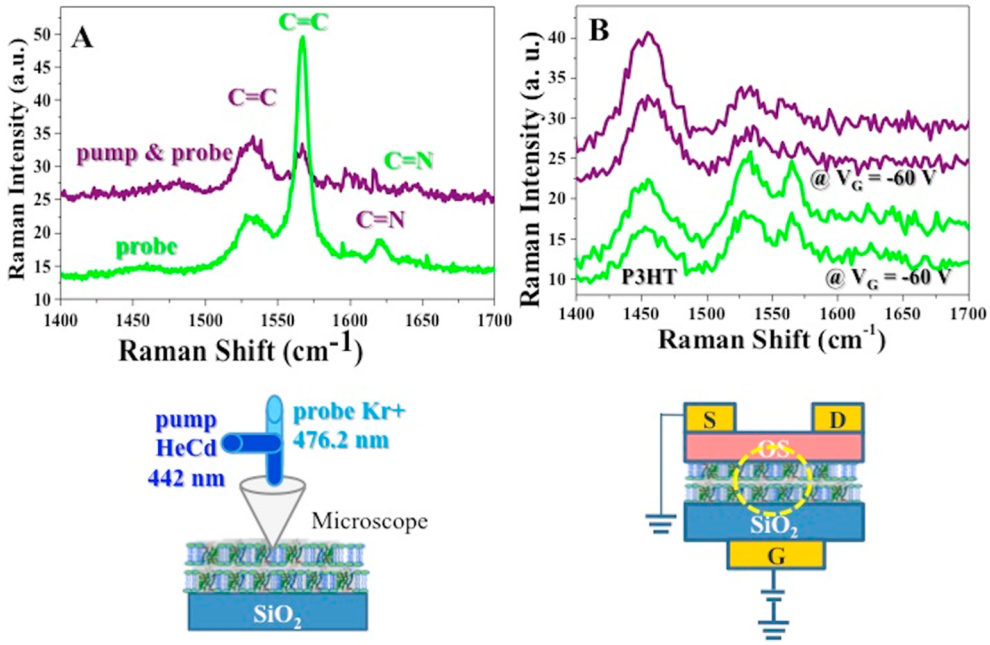

Figure 5. Raman spectra measured in the pump and probe experimental setting illustrated in the main text. Kr^+ laser (476.2 nm) is the probing, while the HeCd (442 nm) is the pumping beam. (A) Raman spectra of a PM film deposited on a SiO_2 substrate with the sole probing beam (green line) and with both pump and probe beams (purple line). (B) Raman spectra measured on the PM FBI-OFET device; green and purple color codes are as for panel (A). The curves measured under a gate bias of −60 V are labeled.

resonant Raman spectra of the bR protein in its two conformational states (dark and light adapted), a pump and probe measuring setup was implemented.[31,32] The Kr^+ laser radiation at 476.2 nm was chosen, as the probing beam is close to the PM isosbestic point at 460 nm. Indeed the radiation at 476.2 nm promotes the transition from the bR_{568} to the M_{412} forms and acts, though weakly, as a "green-yellow" source. As pump, the He−Cd blue line at 442 nm was used. These photons, according to Scheme 1, trigger the M_{412} form and switch it back to the bR_{568} state.

Figure 5A compares typical Raman spectra of the dry PM film deposited on the Si/SiO_2 substrate and measured under exposure to only the Kr^+ laser probing beam (green line) or to the simultaneous illumination by the Kr^+ probe and He−Cd pump beams (purple line). During the exposure to only the Kr^+ laser, the characteristic Raman bands at 1531, 1568, 1643, and 1621 cm^{-1} ascribable to the C═C and the C═N stretching vibrations of the bR_{568} and the M_{412} forms, respectively, are observed.[33] The peak intensity ratio $I_{1531}/I_{1568} \approx 0.2$ (green line) has the value expected for the M_{412} intermediate, demonstrating how the probe radiation switches the bR proteins from the bR_{568} to the M_{412} form, although the process does not proceed thoroughly (the bR_{568} spectral features are still present), as expected being the excitation close to the isosbestic point. When the PM is exposed to both Kr^+ and He−Cd lasers, the intensity of the Raman bands at 1568 cm^{-1} decreases so that the I_{1531}/I_{1568} ratio becomes ∼1.1 (purple line), demonstrating how the beam at 442 nm efficiently pumps back the protein to the purple bR_{568} form.

Figure 5B shows analogous pump-and-probe experiments performed on the PM FBI-OFET device. For this experiment the FBI-OFET was cleaved transversally to the S and D pads and the exciting beam was focused in a ∼1 μm diameter spot, through the microscope objective, onto the area highlighted in the device structure. The purple and green spectra were recorded in exciting configurations similar to those for the homologous spectra in Figure 5A. The feature recorded at 1454 cm^{-1} is the C═C of the P3HT. The two sets of curves marked by the same color are measured either with no applied gate bias or while an applied $V_G = -60$ V drives the device in the whole accumulation mode. The excitation with the sole probe radiation (green trace) sees a $I_{1531}/I_{1568} \approx 1$, showing that in this case the deprotonated species are not predominant. The spectrum recorded with both the pump and probe excitation (purple trace) shows an intensity ratio $I_{1531}/I_{1568} \approx 1.1$, similar to the case of the sole PM layer. Features akin to those recorded with no bias are seen when the gate bias is applied. This is indeed expected under the pump excitation as the bR proteins are already mostly in the deprotonated form. The invariance of the signal as the bias is applied in the presence of both the pump and the probe shows, on the other hand, that in this condition the electric field is indeed not able to produce any isomeric switch. Also no charge was observed in the Raman measurements performed in the presence of halothane, carried out

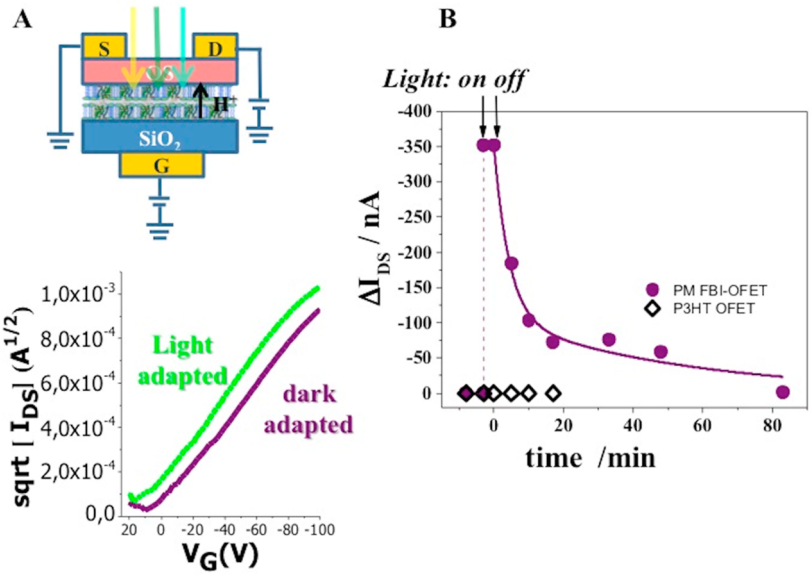

Figure 6. (A) PM FBI-OFET structure under illumination with green-yellow light. (B) Square root of $|I_{DS}|$ − V_G curves at V_{DS} = −80 V measured in the dark (purple curve) or under green-yellow light illuminations (green curve). Illumination conditions are as reported in Figure 4. (C) I_{DS} recovery kinetics after switching the green-yellow light off. Differential I_{DS} values are measured in the dark and under illumination on a PM FBI-OFET as well as on a P3HT OFET.

with the sole probe exciting line, in the absence and in the presence of the electric field. This last evidence confirms that also the exposure to the general anesthetic does not seem to involve an isomeric switch.

Electronic Detection of Photoinduced Proton Translocation. The electronic detection of the bR photoinduced conformational change was investigated by exposing the PM FBI-OFET to green-yellow light (λ > 500 nm) while measuring the OFET $I-V$. In Figure 6A the square root of I_{DS} *vs* V_G at fixed V_{DS} measured in the dark and under green-yellow light illuminations is reported. At all gate biases, the current flowing between source and drain increases its intensity upon illumination, and such an effect was not seen on the bare P3HT OFET. Photocurrents have already been observed for bR sandwiched between two electrodes and are usually ascribed to H^+ pumped upon illumination.[34] However, when bRs are not oriented, a negligible or absent net photocurrent is reported as expected for randomly oriented PM leaflets.[27] We ascribe the observed light-induced increase of I_{DS} to the presence of the negative gate-bias that blocks the H^+ flux in the direction opposite the applied field, leading to a net proton injection into the organic semiconductor. Eventually I_{DS} increases, V_T shifts toward positive values (more than 10 V in Figure 6A), while mobility stays constant, as it can be seen from the green and purple curves being parallel to each other. These experimental evidence support the occurrence of a proton injection from the PM layer into the P3HT OFET channel, causing a whole current increase due to a doping effect of the organic semiconductor.[35]

In Figure 6B the I_{DS} recovery kinetics after switching the green-yellow light off was studied by measuring the OFET transfer characteristics at different time intervals. Data taken on the P3HT OFET are reported for comparison. The differential I_{DS} values at different time lapses are plotted for the PM FBI-OFET. Specifically, I_{DS} is measured at V_{DS} = −80 V and V_G = −100 V; the value measured in the dark *before* the illumination was taken as reference. Upon illumination, ΔI_{DS} jumps to −350 nA as I_{DS} increases. The light is then switched off and the I_{DS} data are taken at regular time lapses as the system relaxes (Figure 6B). It is observed that I_{DS} current decreases according to a two-phase decay that can be modeled with a two-exponential decay. The fast phase, accounting for 70% of the decay, has a characteristic time of hundreds of seconds (240 ± 120 s), compatible with the slow relaxation process observed in the PM absorption spectrum (Figure 3B). The time resolution of these experiments does not allow probing the fast (tens of seconds) phase observed in the absorbance measurements. In addition, there is a significant (30%) very slow decay of the I_{DS} current (several tens of minutes) that can account for the dedoping process of the organic semiconductor involving slow release trap states. Importantly, when the bare P3HT OFET is probed, none of these effects are seen.

It could be argued that the current increase seen in Figure 6 is due to a bare photoexcitation rather than to the proton photopumping occurring in the PM. To clarify this issue and to further characterize the photopumping process and its electronic detection, the experiment reported in Figure 7 was designed. Here a correlation between the differential I_{DS} currents and

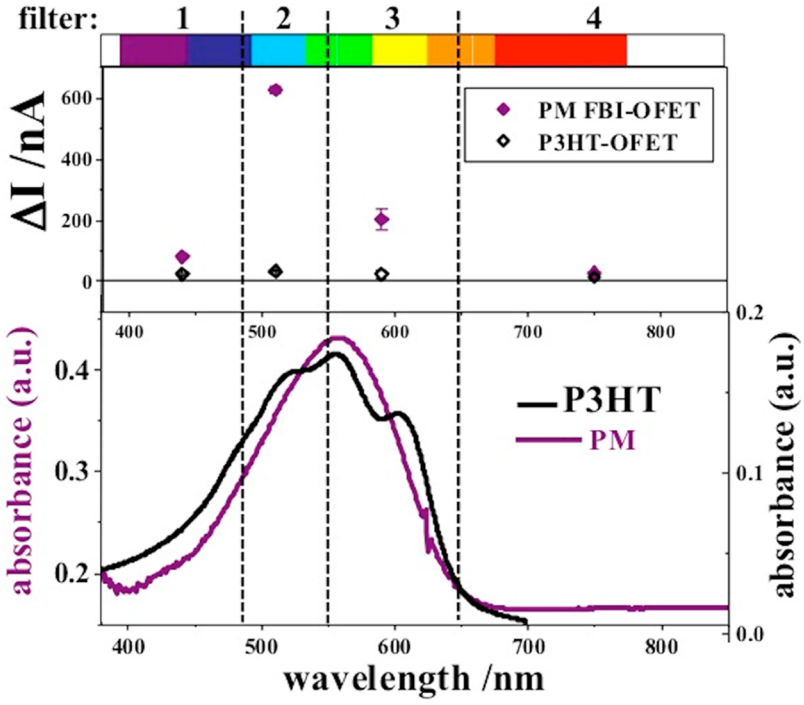

Figure 7. Lower panel shows the absorption spectra of both a PM and a P3HT film. The upper panel compares the PM FBI-OFET and P3HT OFET differential I_{DS} currents measured under exposure to light and in the dark. ΔI (I_{DS} light $-$ I_{DS} dark) variations are reported for light with different wavelengths. To this aim, the following filters were used: filter 1 to select wavelengths in the 390−480 nm range; filter 2 selecting in the range 490−550 nm; and filter 3 for the 550−650 nm range; wavelengths above 680 nm were obtained using filter 4. The data are averaged over three replicates, and the error bars, taken as standard deviations, are reported.

the wavelength of the exciting light is established. To this end, the current responses of a bare P3HT-OFET and a PM FBI-OFET are measured upon illumination with different wavelengths (filter wavelength ranges as indicated in the top axis of Figure 7). The differential I_{DS} current values ($\Delta I = I_{light} - I_{dark}$, taken at $V_{DS} = -80$ V and $V_G = -100$ V) were normalized for the different light intensities and are reported in the upper panel of Figure 7, while the adsorption spectra of the PM and P3HT films are reported in the lower panel. The bR response in terms of photoinduced proton pumping power is very different above and below 500 nm: blue-green light ($\lambda < 490$ nm) inhibits the proton translocation, while green-yellow light ($\lambda > 500$ nm) promotes this process.[2] Indeed, when the green-yellow component of the source spectrum (filters 2 and 3) is shined on the PM FBI-OFET, a net increase in I_{DS} is seen; much less pronounced (if any) is the effect on the P3HT OFET. The photoinduced current drops when light with $\lambda >$ 680 nm is used (filter 4), and, importantly, the light-induced changes in the source−drain current vanish under blue light ($\lambda < 490$ nm, filter 1) illumination. The blue light drives the protein back to the bR_{568} fundamental state (see Scheme 1), thus switching any proton pumping activity off.[2] Such an occurrence proves that the effect seen with the green-yellow light is unambiguously associated with the photoinduced proton-pumping function of the bR. These evidence support a model of H^+ ions photogenerated in the bR and injected from the PM directly into the OFET P3HT channel. The experiments also confirm that both the isomer and the Schiff-base protonation switches occur at the molecular level. It is also a clear evidence of electronic detection of the proton translocation process occurring in bR protein upon absorption, and, indeed, if homogeneously oriented PM patches were used, a much larger current increase would have been seen.

Electronic Detection of Halothane-Triggered Proton Translocation. The proton translocation process in bR is known to be influenced by the presence of exogenous chemical compounds such as volatile general anesthetics.[8] The interactions between anesthetics and membrane proteins (ion channels and receptors) are, indeed, actively investigated,[36] and bR, being a robust prototype for membrane proteins, is among the studied systems. Its absorbance spectrum and photoreactivity are also known to be influenced by anesthetics, but the electronic detection of these effects has not been reported by other groups, so far. Along this line the PM FBI-OFET response to halothane vapors in a N_2 atmosphere has been investigated, and the electronic responses are reported in Figure 8A as an increase in the I_{DS} current upon exposure to 5% halothane. Differently from previous reports, all the measurements involving anesthetic vapors are carried out in the dark. In Figure 8B the dose curves of the PM FBI-OFET compared to that of the P3HT-OFET are reported as relative

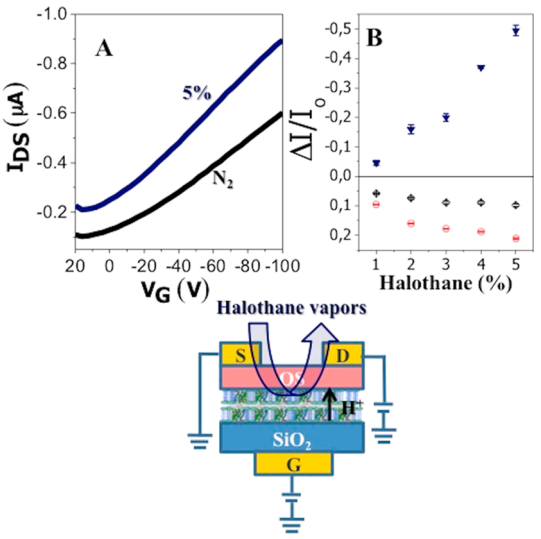

Figure 8. Halothane responses of PM FBI-OFETs. (A) $I_{DS}-V_G$ curves at $V_{DS} = -80$ V measured in an inert N_2 flux (black curve) and in a 5% halothane atmosphere (blue curve). (B) Responses of PM-FBI-OFET (blue triangles), P3HT-OFET (black diamonds), and PL-FBI-OFET (red circles) to clinically relevant halothane concentrations. Values are reported as averages over three replicates, and error bars are the standard deviations. The highly reversible interaction allowed measuring the response to all the concentrations on the same device.

current variations upon exposure to halothane in the 1−5% concentration range. The effect of the halothane interaction with the PM FBI-OFET is opposite of that observed in the case of the bare P3HT OFET, where a very weak current decrease is detected. Interestingly, a small current decrease has been reported also when a phospholipid (PL) FBI OFET is exposed to halothane.[15] Therefore, the effect of the PM interaction with halothane can be ascribed to the bR rather than to the phospholipids present in the PM or to the P3HT. The interfacial nature of the electronic detection is proven by the independence of the response from the PM layer thickness. Incidentally, it is also worth noting that the halothane detection is achieved at very low concentrations comparable to clinically relevant ones.

As already anticipated, the effects of volatile anesthetics on the structure of bRs in the PM have been so far studied mostly by spectroscopic investigation.[7] Depending on the concentration of volatile anesthetics, three modes of interaction with the PM have been found.[37] Very large concentrations of anesthetics irreversibly remove the retinal from the bR interior, leading to the loss of photoactivity and a parallel deep blue shift of the PM absorption maximum to 380 nm. The reversible shift of the PM absorption maximum from 568 to 480 nm, upon exposure to moderate concentrations of halothane, enflurane, and methoxyflurane vapors, has been the subject of several investigations.[7,8,37] These studies assessed that an acid−base equilibrium exists between native bR and the form absorbing at 480 nm, the latter being unable to pump protons although having a long-living *M*-intermediate. Actually, the exposure to these anesthetic concentrations increases the 13-*cis*- to *all-trans*-retinal ratio. Finally, at the very low anesthetic concentrations used in clinical practice as well as in the present study, the efficiency of the proton pump is enhanced, the *M*-intermediate becomes short living (compared to the native state), and only subtle modifications in the spectrum are observed (2 nm blue shift in the maximum).

A useful aid to the understanding of the mechanism by which the bR in the PM FBI-OFET responds to the presence of anesthetic vapors comes from the reports on the electric-field-induced Schiff-base deprotonation measured in the dark.[38,39] Here a mutant bacteriorhodopsin endowed with a weaker binding of the Schiff-base proton (p*K* of approximately 9, as opposed to a p*K* value of 13 in the wild-type bR) is used to demonstrate that a deprotonation of the Schiff base is achieved in the dark, upon application of an external electric field. In light of these findings, the PM FBI-OFET behavior can be explained considering that the general anesthetic molecules (halothane specifically) change the pK_a of the Schiff base, favoring its deprotonation to an extent that, in the presence of a strong enough electric field, proton translocation occurs. In the present work, the role played by the site-specific mutation is played by the anesthetic molecules capable of tuning the affinity of the intraprotein Schiff base for the protons and finally allowing H^+ injection into the p-type channel by means of the applied gate-field.

These findings allow us to assess that the molecular switching mechanism governing the interaction with anesthetics is indeed the amino acid protonation switch, while, differently from what was previously published,[8] no isomer switch seems to occur. This is also confirmed by the fact that Raman spectral changes were not seen in the presence of anesthetics even under bias.

CONCLUSIONS

A p-type OFET embedding bR nanolamellae is used to detect proton translocation processes occurring when the device is exposed either to green-yellow light or to anesthetic vapors. In both cases the effect is a current increase detected with the functional-biointerlayer OFET. Protons generated upon exposure to the two different external stimuli are indeed injected into the p-type organic semiconductor due to the direct electronic/ionic coupling existing between the biolayer and the OFET channel. This work shows that, though characterized by the same electronic effect, the two proton translocations underpin different molecular switching processes. While photoexposure gives rise to both a photoinduced isomerization and a deprotonation of the Schiff-base linkage, the

anesthetic molecules generate an amino acid protonation switch. This knowledge could be reached thanks to the FBI-OFET device, which allowed detecting both stimuli with the very same electronic device.

METHODS

Materials. Dry, lyophilized purple membranes (Munich Innovative Biomaterials GmbH) dispersed in distilled water (3 mg/mL) formed a uniform suspension after a mild sonication on ice (5 cycles of 5 s with 2 min interval). This suspension is diluted in water to a concentration of 10 μg/mL, and 60 μL was spin-coated at 150 rpm for 90 min directly on the cleaned SiO_2 surface or on glass. The 10 μg/mL PM suspension resulted in a 1 μm thick film, while lower PM concentrations resulted in proportionally thinner films. Unless otherwise stated, the 1 μm thick PM film was used.

Highly regioregular poly(3-hexylthiophene-2,5-diyl) (RR >98%, BASF Sepiolid P200) was purified[40] and dissolved in chloroform at a concentration of 2.6 mg/mL. The solution absorption spectrum was dominated by a single band centered at 452 nm, while the solid-state spectrum of purified P3HT features three vibronic bands located at 520, 555, and 602 nm. Both these evidence are consistent with a (average) high molecular weight of *ca.* 10 kDa.[41] A P3HT chloroform solution was spin-coated at a spin rate of 2000 rpm for 30 s, resulting in a P3HT film thickness of about 20 nm.

FBI-OFET Device Fabrication Procedure. The devices were fabricated starting from a highly n-doped silicon substrate acting as the gate contact covered by a 300 nm thick thermally grown SiO_2 gate dielectric exhibiting a capacitance per unit area (C_i) of 12 nF/cm^2. The PM capturing layer was spin deposited on the SiO_2 surface, previously cleaned through a rinsing procedure involving treatment with solvents of increasing polarity.[42] The measured PM-SiO_2 stacking layers' capacitance per unit area does not differ significantly from that of the bare SiO_2, as the PM layer holds a comparatively much higher capacitance. The P3HT p-type semiconductor was deposited directly over the PM layer. Source, drain. and gate contacts were defined by thermal evaporation in a vacuum (8×10^{-7} Torr) of gold through a shadow mask reproducing a sequence of 38 rectangular pads with a width (W) of 4 mm and spaced by $L = 200$ μm (channel length). In Figure 1A a cross-sectional schematic of the device structure is provided.

Electronic Response Measurements. The electronic responses of the OFET exposed to an external stimulus (light or gaseous halothane at a concentration in the 1−5% range in N_2) have been acquired by measuring the OFET drain-source current−gate-source voltage ($I_{DS}-V_G$) transfer characteristics while keeping the source−drain bias, V_{DS}, fixed at −80 V. The transfer characteristic baseline was measured in an inert atmosphere (N_2 or darkness for gas and the light-sensing measurements, respectively) and in the presence of the external stimulus. All the measurements of the vapor atmosphere are carried out in the dark. The response ($\Delta I/I_0$) was evaluated as

$$[I(I_{DS} \text{ upon expos. to ext. stim.}) - I_0(I_{DS} \text{ in inert atmos.})]/I_0 \quad (3)$$

The I_0 and I values are taken at $V_G = -100$ V. The $\Delta I/I_0$ is the electronic response at a given concentration, and the relevant dose curve is obtained by plotting the data points at all investigated concentrations as the average values over three replicates, while the error bars are taken as the standard deviation. The halothane interaction with the PM layer is reversible, and this allows performing all the measurements on the same device. A flux of controlled concentration of halothane vapors in N_2 was obtained by bubbling the N_2 carrier gas into two bubblers connected in series containing the liquid halothane. This allows obtaining a nitrogen flow having a partial pressure of halothane vapor equal to its saturated vapor pressure at the working temperature. This was controlled by dipping the bubblers into a cryothermostat bath, while the control of the flow was achieved through a system of two computer-controlled flowmeters (Brooks Smart DMFC model 5850C). The described experimental apparatus allows controlling independently and simultaneously the flow of the carrier gas and that of the nitrogen saturated with the analyte. Different analyte concentrations were obtained therefore by subsequent dilutions, changing the rate of the two flows. The analyte concentrations were delivered in a random sequence, and all the measurements were carried out in the dark. With this apparatus, I_0 was evaluated by measuring the transfer characteristics of the OFET sensor in a N_2 flux or in the dark. Afterward, on the same device, a controlled concentration flow of halothane was delivered and the I_D current was measured. The same procedure was performed to evaluate the OFET response under illumination.

Morphological and Optical Characterization. The PM and P3HT film morphology was inspected by means of AFM on an XE-100E (Park System Corp., Korea) in noncontact mode using silicon tips (curvature radius <10 nm, force constant 40 N/m).

By means of UV−visible absorption spectroscopy, the effect of light on the absorption spectrum of PM was assessed. To this aim, an Agilent 8453 diode array spectrophotometer was used. The full spectrum from 190 to 1100 nm was recorded within 1 s with a spectral resolution of 1 nm. The PM-P3HT film, deposited on glass, was placed at 45° to allow illumination with both the measuring beam and the exciting green-yellow light (supplied by a cold light source, filtered through a filter, $\lambda > 500$ nm; density power on the sample was about 1.86 mW/cm^2). The following other filters were used: filter 1, selecting wavelengths in the 390−480 nm range; filter 2, 490−550 nm; filter 3, 550−650 nm; while wavelengths above 680 nm are selected with filter 4.

GISAXS measurements were carried out with a S3-MICRO SWAXS camera system (HECUS X-ray Systems, Graz, Austria) on PM or P3HT-PM films deposited on Si/SiO_2. Cu Kα radiation of wavelength $\lambda = 1.542$ Å was provided by an ultrabrilliant point microfocus X-ray source (GENIX-Fox 3D, Xenocs, Grenoble), operating at a maximum power of 50 W (50 kV and 1 mA). The sample-to-detector distance was 269 mm. The volume between the sample and the detector was kept under vacuum during the measurements to minimize scattering from the air. The Kratky camera was calibrated in the small-angle region using silver beneath ($d = 58.38$ Å).[43] Scattering curves were obtained in the Q-range between 0.01 and 0.54 Å^{-1}, q being the scattering vector [$q = (4\pi/\lambda) \sin\theta$] and 2θ the scattering angle. The scattered intensities can be recorded in the q_z and q_r directions (in-plane and out-of plane scattering). A 1D-PSD-50 M detector (HECUS X-ray Systems) containing 1024 channels of width 54.0 μm and oriented perpendicular to the wafer plane was used for the wafer alignment and for the detection of scattered signal only in the out-of-plane direction.

The Raman spectra were obtained by focusing the 476.2 nm line of the Kr^+ probe and 442 nm of the HeCd pump laser onto the surface of the PM deposited on the Si/SiO_2 substrate to a spot of 1 μm diameter using an 80× microscope objective. The sample position relative to the Kr^+ and HeCd laser spot was controlled by a piezoelectric $x-y$ stage with a step of 0.1 mm. The Rayleigh scattering generated by the laser light was suppressed using an interference notch filter. Laser-induced overheating of the samples was minimized by keeping the incident power density below 1.3×10^4 W/cm^2. The Raman signal was dispersed using a 0.64 m monochromator and finally detected using a Si charge coupled device detector cooled to 140 K.

Conflict of Interest: The authors declare no competing financial interest.

Acknowledgment. We acknowledge funding from FlexSMELL (Gas Sensors on Flexible Substrates for Wireless Applications, FP7-PITN-GA-2009-238454), OrgBio (Organic Bioelectronics,

FP7-ITN-People-GA-2013-607896), and PON LABORATORIO SISTEMA (Laboratorio per lo Sviluppo Integrato delle Scienze e delle Tecnologie dei Materiali Avanzati e per dispositivi innovativi), Italian Ministry of Education, University and Research (MIUR). E.F., G.P., and F.R. acknowledge financial support from Consorzio Interuniversitario per lo Sviluppo dei Sistemi a Grande Interfase (CSGI) and the Italian Ministry of Education, University and Research (MIUR).

REFERENCES AND NOTES

1. Oesterhelt, D.; Stoeckenius, W. Functions of A New Photoreceptor Membrane. *Proc. Natl. Acad. Sci. U.S.A.* **1973**, *70*, 2853–2857.
2. Haupts, U.; Tittor, J.; Oesterhelt, D. Closing in on Bacteriorhodopsin: Progress in Understanding the Molecule. *Annu. Rev. Biophys. Biomol. Struct.* **1999**, *28*, 367–99.
3. Lozier, R. H.; Bogomolni, R. A.; Stoeckenius, W. Bacteriorhodopsin: A Light-Driven Proton Pump of Halobacterium Halobium. *Biophys. J.* **1975**, *15*, 955–962.
4. Varo, G.; Lanyi, J. Distortions in the Photocycle of Bacteriorhodopsin at Moderate Dehydration. *Biophys. J.* **1991**, *59*, 313–322.
5. Tóth-Boconádi, R.; Dér, A.; Keszthelyi, L. Optical and Electric Signals from Dried Oriented Purple Membrane of Bacteriorhodopsins. *Bioelectrochemistry* **2011**, *81*, 17–21.
6. Hampp, N. Bacteriorhodopsin as a Photochromic Retinal Protein for Optical Memories. *Chem. Rev.* **2000**, *100*, 1755–1776.
7. Boucher, F.; Taneva, S. G.; Elouatik, S.; Déry, M.; Messaoudi, S.; Harvey-Girard, E.; Beaudoin, N. Reversible Inhibition of Proton Release Activity and the Anesthetic-Induced Acid-Base Equilibrium between the 480 and 570 nm Forms of Bacteriorhodopsin. *Biophys. J.* **1986**, *70*, 948–961.
8. Nishimura, S.; Mashimo, T.; Hiraki, K.; Hamanaka, T.; Kito, Y.; Yoshiya, I. Volatile Anesthetics Cause Conformational Changes of Bacteriorhodopsin in Purple Membrane. *Biochim. Biophys. Acta, Biomembr.* **1985**, *818*, 421–424.
9. Sharmar, P.; Roy, S. All-Optical Biomolecular Parallel Logic Gates with Bacteriorhodopsin. *IEEE Trans. Nanobiosci.* **2004**, *3*, 129–136.
10. Renner, T.; Hampp, N. Bacteriorhodopsin-Films for Dynamic Time Average Interferometry. *Opt. Commun.* **1993**, *96*, 142–149.
11. Cullin, D. W.; Vsevolodov, N. N.; Dyukova, T. V. Holographic Properties of Triton X-100-Treated Bacteriorhodopsin Embedded in Gelatin Films. *Biosystems* **1995**, *35*, 141–144.
12. Birge, R. R.; Gillespie, N. B.; Izaguirre, E. W.; Kusnetzow, A.; Lawrence, A. F.; Singh, D.; Song, Q. W.; Schmidt, E.; Stuart, J. A.; Seetharaman, S.; *et al*. Biomolecular Electronics: Protein-Based Associative Processors and Volumetric Memories. *J. Phys. Chem. B* **1999**, *103*, 10746–10766.
13. Jin, Y.; Honig, T.; Ron, I.; Friedman, N.; Sheves, M.; Cahen, D. Bacteriorhodopsin as an Electronic Conduction Medium for Biomolecular Electronics. *Chem. Soc. Rev.* **2008**, *37*, 2422–2432.
14. Angione, M. D.; Cotrone, S.; Magliulo, M.; Mallardi, A.; Altamura, D.; Giannini, C.; Cioffi, N.; Sabbatini, L.; Fratini, E.; Baglioni, P.; *et al*. Interfacial Electronic Effects in Functional Biolayers Integrated Into Organic Field-Effect Transistors. *Proc. Natl. Acad. Sci. U.S.A.* **2012**, *109*, 6429–6434.
15. Angione, M. D.; Magliulo, M.; Cotrone, S.; Mallardi, A.; Altamura, D.; Giannini, C.; Cioffi, N.; Sabbatini, L.; Gobeljic, D.; Scamarcio, G.; *et al*. Volatile General Anesthetic Sensing with Organic Field-Effect Transistors Integrating Phospholipid Membranes. *Biosens. Bioelectron.* **2013**, *40*, 303–307.
16. Magliulo, M.; Mallardi, A.; Gristina, R.; Ridi, R.; Sabbatini, L.; Cioffi, N.; Palazzo, G.; Torsi, L. Part-per-Trillion Label-Free Electronic Bio-Analytical Detection. *Anal. Chem.* **2013**, *85*, 3849–3857.
17. Macchia, E.; Giordano, F.; Magliulo, M.; Palazzo, G.; Torsi, L. An Analytical Model for Bio-Electronic Organic Field-Effect Transistor Sensors. *Appl. Phys. Lett.* **2013**, *103*, 103301.
18. Dodabalapur, A.; Torsi, L.; Katz, H. E. Organic Transistors: Two-Dimensional Transport and Improved Electrical Characteristics. *Science* **1995**, *268*, 270–271.
19. Torsi, L.; Dodabalapur, A.; Lovinger, A. J.; Katz, H. E.; Ruel, R.; Davis, D. D.; Baldwin, K. W. Synthesis, Material Properties and Transistor Performance of Highly Pure Thiophene Oligomers. *Chem. Mater.* **1995**, *7*, 2247–2251.
20. Angione, M. D.; Pilolli, R.; Cotrone, S.; Magliulo, M.; Mallardi, A.; Palazzo, G.; Sabbatini, L.; Fine, D.; Dodabalapur, A.; Cioffi, N.; *et al*. Carbon Based Materials for Electronic Bio-Sensing. *Mater. Today* **2011**, *14*, 424–433.
21. Torsi, L.; Magliulo, M.; Manoli, K.; Palazzo, G. Organic Field-Effect Transistor Sensors: A Tutorial Review. *Chem. Soc. Rev.* **2013**, *42*, 8612–8628.
22. Torsi, L.; Dodabalapur, A. Organic Thin-Film Transistors as Plastic Analytical Sensors. *Anal. Chem.* **2005**, *77*, 380A–387A.
23. Shen, Y. I.; Safinya, C. R.; Liang, K. S.; Ruppert, A. F.; Rothschild, K. J. Stabilization of the Membrane Protein Bacteriorhodopsin to 140 °C in Two-Dimensional Films. *Nature* **1993**, *366*, 48–50.
24. Cho, S.; Lee, K.; Yuen, J.; Wang, G.; Moses, D.; Heeger, A. J.; Surin, M.; Lazzaroni, R. Thermal Annealing-Induced Enhancement of the Field-Effect Mobility of Regioregular Poly(3-hexylthiophene) Films. *J. Appl. Phys.* **2006**, *100*, 114503.
25. Torsi, L.; Dodabalapur, A.; Lovinger, A. J.; Katz, H. E.; Ruel, R.; Davis, D. D.; Baldwin, K. W. Rapid Thermal Processing of α-Hexathienylene Thin-Film-Transistors. *Chem. Mater.* **1995**, *7*, 2247–2251.
26. Lovinger, J.; Davis, D. D.; Dodabalapur, A.; Katz, H. E.; Torsi, L. Single-Crystal and Polycrystalline Morphology of the Thiophene-Based Semiconductor α-Hexathienyl (α-6T). *Macromolecules* **1996**, *29*, 4952–4957.
27. Povilas-Kietis, B.; Saudargas, P.; Varo, G.; Valkumas, L. External Electrical Control of the Proton Pumping in Bacteriorhodopsin. *Eur. Biophys. J.* **2007**, *36*, 199–221.
28. Sikora, S.; Little, A. S.; Dewey, T. G. Room Temperature Trapping of Rhodopsin Photointermediates. *Biochemistry* **1994**, *33*, 4454–4459.
29. Francia, F.; Palazzo, G.; Mallardi, A.; Cordone, L.; Venturoli, G. Probing Light-Induced Conformational Transitions in Bacterial Photosynthetic Reaction Centers Embedded in Trehalose Amorphous Matrices. *Biochim. Biophys. Acta Bioenergetics* **2004**, *1658*, 50–57.
30. Braga, D.; Horowitz, G. High-Performance Organic Field-Effect Transistors. *Adv. Mater.* **2009**, *21*, 1473–1486.
31. Aton, B.; Doukas, A. G.; Callender, R. H.; Becher, B.; Ebrey, T. G. Resonance Raman Studies of the Purple Membrane. *Biochemistry* **1977**, *16*, 2995–2999.
32. Terner, J.; Campion, A.; El-Sayed, M. A. Time-Resolved Resonance Raman Spectroscopy of Bacteriorhodopsin on the Millisecond Timescale. *Proc. Natl. Acad. Sci. U.S.A.* **1977**, *74*, 5212–5216.
33. Stockburger, M.; Klusmann, W.; Gattermann, H.; Massig, G.; Peters, R. Photochemical Cycle of Bacteriorhodopsin Studied by Resonance Raman Spectroscopy. *Biochemistry* **1979**, *18*, 4886–4900.
34. Koyama, K.; Yamaguchi, N.; Miyasaka, T. Antibody-Mediated Bacteriorhodopsin Orientation for Molecular Device Architectures. *Science* **1994**, *265*, 762–765.
35. Herlogsson, L.; Crispin, X.; Robinson, N. D.; Sandberg, M.; Hagel, O. J.; Gustafsson, G.; Berggren, M. Low-Voltage Polymer Field-Effect Transistors Gated *via* a Proton Conductor. *Adv. Mater.* **2007**, *19*, 97–101.
36. Vemparala, S.; Domene, C.; Klein, M. L. Computational Studies on the Interaction of Inhalation Anesthetics and Proteins. *Acc. Chem. Res.* **2010**, *43*, 103–110.
37. Nakagawa, T.; Hamanaka, T.; Nishimura, S.; Uchida, I.; Mashimo, T.; Kito, Y. The Quantitative Analysis of the Three Action Modes of Volatile Anesthetics on the Purple Membranes. *Biochim. Biophys. Acta* **2000**, *1467*, 139–149.
38. Kolodner, P.; Lukashev, E. P.; Ching, Y.-C.; Rousseau, D. Electric-Field-Induced Schiff-Base Deprotonation in D85N

Mutant Bacteriorhodopsin. *Proc. Natl. Acad. Sci. U.S.A.* **1996**, *93*, 11618–11621.
39. Kolodner, P.; Lukashev, E. P.; Ching, Y. C. Electric-Field Effects in Dry Films of D85N and D85, 96N Mutant Bacteriorhodopsin. *Bioelectrochemistry* **2000**, *51*, 67–73.
40. Urien, M.; Wantz, G.; Cloutet, E.; Hirsch, L.; Tardy, P.; Vignau, L.; Cramail, H.; Parnei, J. P. Field-Effect Transistors Based on Poly(3-hexylthiophene): Effect of Impurities. *Org. Electron.* **2007**, *8*, 727.
41. Verilhac, J. M.; LeBlevennec, G.; Djurado, D.; Rieutord, F.; Chouiki, M.; Travers, J. P.; Pron, A. Effect of Macromolecular Parameters and Processing Conditions on Supramolecular Organisation, Morphology and Electrical Transport Properties in Thin Layers of Regioregular Poly(3-hexylthiophene). *Synth. Met.* **2006**, *156*, 815–823.
42. Dinelli, F.; Moulin, J. F.; Loi, M. A.; Da Como, E.; Massi, M.; Murgia, M.; Muccini, M.; Biscarini, F. Effects of Surface Chemical Composition on the Early Growth Stages of α-Sexithienyl Films on Silicon Oxide Substrates. *J. Phys. Chem. B* **2006**, *110*, 258–263.
43. Blanton, T. N.; Huang, T. C.; Toraya, H.; Hubbard, C. R.; Robie, S. B.; Louer, D.; Gobel, H. E.; Will, G.; Gilles, R.; Raftery, T. JCPDS - International Centre for Diffraction Data Round Robin Study of Silver Behenate. A Possible Low-Angle X-Ray Diffraction Calibration Standard. *Powder Diffr.* **1995**, *10*, 91–95.